Supplementary material to the paper: "Markers of the pyroxenite contribution in the major-element compositions of oceanic basalts: review of the experimental constraints" by Sarah Lambart, Didier Laporte and Pierre Schiano

Appendix 1: Experimental and analytical methods

A1.1. Starting materials

We used fine powders of natural pyroxenites M5-40 and M7-16 from the Beni Bousera ultramafic massif (Table S1). M5–40 is a garnet websterite, which plots very close to the mean of the pyroxenite worldwide population. Sample M7–16 is a garnet–olivine clinopyroxenite; compared to M5–40, it is depleted in SiO_2 and Na_2O, and enriched in FeO, CaO, and TiO_2. Both pyroxenites are olivine normative and silica-deficient (see text; Kogiso et al., 2004; Schiano et al., 2000), but they show different degrees of silica undersaturation: M7-16 is nepheline (Ne) normative (2.3%) and M5-40 is hypersthene (Hy) normative (8.3%).

Both pyroxenites were crushed in an agate mortar, and then ground under ethanol in an agate micronizing mill to reduce the grain size to 2-4 μm. Rock powders were fired for 6 h at 900 °C in a CO_2/H_2 atmosphere with an oxygen fugacity between the magnetite–wüstite and iron-wüstite buffers (f_{O_2} = $10^{-15.91}$ bar). The starting materials were stored under vacuum to reduce water adsorption.

A1.2. Experimental techniques

All experiments, except #40-L3 (see below), were made in an end-loaded, ½-inch piston-cylinder apparatus at the Laboratoire Magmas et Volcans. *P-T* and run durations are summarized in Table 1. From outside to inside, assemblies consist of a NaCl cell wrapped in a lead foil, a Pyrex cylinder, a graphite furnace. We used double sample capsules made of graphite (inside) and platinum (outside). The graphite container was loaded with 16.9-19.8 mg of starting powder, and then put into the platinum capsule and covered with a graphite lid. The platinum capsule was dried in an oven at 300°C for 24h. Capsules are placed inside the graphite furnace, between a rod and a sheath of crushable MgO, and lie at the hot spot of the assembly. A thin-walled MgO sheath surrounds the capsule to avoid direct contact between the outer platinum container and the graphite furnace. Temperature is controlled by calibrated $W_{95}Re_5/W_{74}Re_{26}$ thermocouple. The thermocouple tip is stuck into the MgO sheath and is separated from the sample capsule by a 0.6-mm thick crushable MgO disc. In all the experiments, the sample was placed at exactly the same height (to within 0.1 mm) into the graphite furnace to ensure good temperature reproducibility. To minimize the amount of adsorbed water, all pieces were fired at high temperature (8h at 1,000°C, then 24h at 400°C for crushable MgO; 1h at 600°C for NaCl; ≈ 24h at 400°C for all other pieces), and then stored at 150°C. Just before an experiment, the full assemblage was fired a last time 24 h at 300°C.

To analyze the composition of liquids in equilibrium with mineral phases, we used the ''microdike'' technique developed by Laporte et al. (2004), which consists of extracting small volumes of liquid into fractures of the graphite container that formed during experiments. This technique, originally designed

for 3/4-inch piston-cylinder assemblies, was adapted to 1/2-inch assemblies by Lambart et al. (2012). The main modification is that the thicknesses of the platinum capsule and of the graphite walls are increased from 0.2 mm and 0.8-0.9 mm in 3/4-inch assemblies to 0.5 mm and 1.1-1.2 mm in 1/2-inch assemblies, respectively (Fig. S1). A few microdikes were observed in all experiments [Fig. 6b; see also Fig. 1 in Lambart et al. (2012)], both at the top and at the bottom of the sample chamber. As the thermal gradient in our assemblies is small (~ 5°C in the sample chamber), liquid compositions are homogeneous throughout the sample chamber and there are no significant differences between glasses analyzed in upper and lower microdikes, as exemplified by sample 40-H3 in Table 1 (see also Lambart et al., 2009a,b). Microdike sizes vary from tens to hundreds of µm in length and from a few µm to hundreds of µm in width. These lengths are smaller than the thickness of the graphite walls making the contact between melt and platinum container very unlikely. Moreover, we measured composition profiles along the biggest dikes (Figs. 6b, S2), and we observed no correlation between the iron content of melt and the distance to the capsule. This observation, combined with the good results of mass balance on iron, shows that our experiments did not suffer iron loss.

Experiment #40-L3 was run in an end-loaded, 1/2-inch piston-cylinder apparatus at the California Institute of Technology using inner pieces of crushable MgO that had been dried at 1000°C, a straight-walled graphite furnace and an outer sleeve of calcium fluoride wrapped in a lead foil. We used a graphite crucible in a platinum capsule [see Baker and Stolper (1994) for more details] but no melt extraction technique was used. The platinum capsule was dried in an oven at 400°C for 3h and then rapidly welded shut while still hot. Temperature was controlled by calibrated $W_{97}Re_3/W_{75}Re_{25}$ thermocouple.

A1.3. Analytical techniques.

At the end of an experiment, the capsule was enclosed in epoxy, sectioned lengthwise, polished and carbon-coated. Textures and phase assemblages were characterized using a JEOL JSM-5910 LV scanning electron microscope. Phase compositions (except for 40-L3) were analyzed with a Cameca SX100 electron microprobe at the Laboratoire Magmas et Volcans. Phase compositions of 40-L3 were analysed with a five-spectrometer JEOL JXA-8200 at Caltech. A 15-kV accelerating voltage, a 15-nA beam current, counting times of 20 s for Ni, Cr and Ti, and of 10 s for other elements, and a focused beam were used for crystalline phases. For glass analyses, the beam current was lowered to 8 nA and a beam size of 5 µm was used to minimize sodium loss. The analytical totals for glasses vary between 94 and 99 wt%. Low analytical totals (between 94 and 97 wt%) were obtained in the case of very thin microdikes, due to beam overlap onto graphite. The proportions of liquid and solid phases best fitting the bulk composition of the starting material were calculated using a mass balance program modified from Albarède & Provost (1977). Table 1 summarizes the experimental conditions and the phase proportions and compositions in the run products.

A1.4. Attainment of equilibrium.

Phase assemblages, modes and run durations are given in Table 1. The durations of our experiments (97-148 h) are significantly longer than those in most high-pressure and high-temperature studies

(Hirschmann et al., 2008). Duplicate experiments (40-C3 and 40-D4; Table 1) attest to the reproducibility of experiments. Although the present set of experiments was not reversed, the following observations indicate that chemical equilibrium was closely approached: (1) Cpx and Ol crystals show no detectable compositional zoning and the compositional variability in a single sample is small; (2) despite the presence of unreacted cores (≤ 5 μm) in some garnets and a more variable composition in a single sample, probably as a result of incomplete equilibration, the sums of squared residuals in mass balance calculations performed with all oxides are low (0.32 in average, with a range of 0.06–0.89), indicating that relict cores represent a negligible fraction of the total mass and the bulk composition was preserved during the experiments; (3) A high degree of microtextural equilibration is observed even at low degrees of melting (Fig. 6a); (4) Fe-Mg exchange coefficients between Cpx and melt and Gt and melt — 0.32 ± 0.03 and 0.50 ± 0.05, respectively (Table 1) — are broadly consistent with those measured in previous pyroxenite partial melting experiments at P ≥ 2GPa (e.g., Keshav et al., 2004; Kogiso and Hirschmann, 2006; Kogiso et al., 2003); (5) temperatures calculated (T_{cal}) on the basis of Cpx-liquid equilibrium (Putirka et al., 1996; 2003) are in good agreement with the experimental (T_{exp}) temperatures (Fig. S3), as the differences T_{cal} - T_{exp} are well within the error of the thermometer (± 45°C; Putirka, 2008). The close approach of chemical equilibrium in our experiments is due to the long run durations and the fine grain size of the starting materials.

A1.5. Determination of melting reactions

Figure S4 presents the evolution of solid phase proportions as a function of melt fraction in partial melting experiments on M5-40 and M7-16 at 2 and 2.5 GPa. The mode of solid phases consumed during the reaction decreases with increasing *F*. In these representations, the slopes of linear regressions, calculated over the interval of stability of a given solid assemblage, are the coefficients of the melting reactions (Baker and Stolper, 1994; Pickering-Witter and Johnston, 2000). At 2 GPa, melting reactions of M5-40 are:

(1) Opx + Plg + Sp + Gt = liq + Cpx *from solidus to Plg-, Sp- and Opx-out*
(2) 0.30 (6) Cpx + 0.70 (7) Gt = 1 liq *from Opx-out to Gt-out*
(3) 1 Cpx = 1 Liq *from Gt-out to liquidus*

Reaction (1) is only qualitative due to the lack of experimental data at very low degrees of melting. It is estimated knowing the subsolidus assemblage (Cpx + Gt + Opx + Sp + Plg) and by analogy with the melting reaction of M5-40 close to the solidus at 1.5 GPa: 0.36 Opx + 0.34 Plg + 0.21 Sp + 0.24 Gt = 1 liq + 0.19 Cpx (the grey symbols in Fig. S4a; Lambart et al., 2009b). As Opx is much more abundant than Plg and Sp, reaction (1) includes in fact (at least) two reactions: the first one leading to the total consumption of Plg and/or Sp, and the subsequent one leading to the disappearance of Opx. Reaction (2), in which the reactant phases are Cpx and Gt, holds from Opx-out to Gt-out. In reaction (3), the liquidus phase, Cpx, is the only phase consumed, so its coefficient is equal to 1. The intersection point between reactions (2) and (3) for Cpx allows us to estimate the melt fraction at which Gt is suppressed from the residual assemblage: *F* = 37.7 wt% (Fig. S4a). This is perfectly consistent with the estimation obtained from the Gt mode *vs F* best-fit line: *F* = 36.6 wt%.

The melting reactions of M5-40 at 2.5 GPa are:

(1) 0.64 (12) Cpx + 0.36 (52) Gt = 1 liq *from solidus to Gt-out*

(2) 1 Cpx = 1 Liq *from Gt-out to liquidus*

Despite the higher uncertainty of reaction coefficients, it is clear that Gt remains stable to a much higher melt fraction at 2.5 GPa ($F \approx 75.0$ wt%) than at 2 GPa.

The melting reactions of M7-16 at 2 GPa are:

(1) 1.58 Gt + 0.18 Ol = 1 liq + 0.56 Cpx + 0.19 Sp *from solidus to Ol-out*

(2) Cpx + Gt = 1 liq ± Sp *from Ol-out to Gt-out*

(3) Cpx + Sp = 1 Liq *from Gt-out to Cpx-out*

The number of experimental data is not sufficient to determine the coefficients for reactions (2) and (3). At 2.5 GPa, the reactions become:

(1) Cpx + Gt + Ol = 1 Liq *from solidus to Ol-out*

(2) 0.48 Cpx + 0.52 Gt = 1 Liq *from Ol-out to Gt-out*

Appendix 2: Fractional crystallization calculations

A2.1. Determination of the composition of the Model Primary Magma (MPM) and of potential temperatures of px-MORB.

The MORB AII107-7 20-3 used to determine the composition of the primary magma is a MgO-rich basalt (10.05 wt%; Table S4). We used the PRIMELT2 software (Herzberg and Asimow, 2008) to determine the composition of the corresponding primary magma. The composition estimate is dependent on model input parameters, which assume that Cpx did not fractionate in the mantle and that, given the high MgO content in melt, Ol is the only crystallizing phase at 0.1 MPa.

Details of the computational method have been given by Herzberg and O'Hara (2002), Herzberg et al. (2007) and Herzberg and Asimow (2008). Briefly, the program calculates a primary magma composition by incremental addition of Ol to bring a lava composition into equilibrium with a given peridotite composition (defined by its Mg#) and can model both batch and accumulated fractional melting. Potential temperatures (T_P) are also calculated from the MgO content of the primary magma composition, using the relation: T_P(°C) = 1463 + 12.74MgO - 2924/MgO (Herzberg and O'Hara, 2002). Estimates on T_P have a precision that is similar to the accuracy of the olivine liquidus temperature (i.e, ±31°C (2σ); Herzberg and Gazel, 2009).

MORB AII107-7 20-3 was run through the PRIMELT2 program assuming a major element composition of the mantle source equal to DMM1 (Wasylenki et al., 2003). The calculated primary magma composition (MPM) was supposed to be derived by accumulated fractional melting of this peridotite. The oxidation state of the source was fixed at $Fe^{2+}/\Sigma Fe$ and Fe_2O_3/TiO_2 ratios of 0.89 and 0.5 respectively. The same procedure and parameters were used to determine the T_P of px-MORB (Table S3).

A2.2. Fractional crystallization

In order to test if the low SiO_2 and high FeO contents of px-MORB can be attributed to fractionation processes, we performed thermodynamic modeling using MELTS (Ghiorso and Sack, 1995) to reproduce a fractional crystallization path at various pressures. MELTS is a thermodynamical program that can model the effect of fractional crystallization on the major element composition of an igneous suite. A detailed description of the workings of MELTS is given in Ghiorso and Sack (1995) and Asimow and Ghiorso (1998). Among other calculations, MELTS software can model crystallization paths under certain temperature, pressure, oxygen fugacity, total enthalpy, total entropy and total volume constraints.

The fractional crystallization paths of MPM (Fig. 11) have been modeled at 0.1 MPa, 100 MPa, 200 MPa, 300 Mpa, and 400 MPa, using 1 °C temperature intervals. Calculations have been performed at f_{O_2} = FMQ - 1 (i.e. the fayalite-magnetite-quartz buffer minus 1). For comparison, we also performed some calculations at FMQ and FMQ-2 and we obtained very similar results. The same procedure has been used to calculate fractionation paths from experimental peridotite and from stage 2 pyroxenite melts at 10 MPa in Figure 14.

Appendix 3: Isobaric melt productivity of pyroxenite MIX1G

Assuming that, for melt fractions (*F)* in excess of 5 wt%, *F* is a quadratic function of temperature (*T*) (Pertermann and Hirschmann, 2003a), the melting function of pyroxenite MIX1G is (Fig. 15a):

F (wt%) = $a \cdot T'^2 + b \cdot T' + 5$ with a = 79.23, b = 14.13, and T' (°C) = $(T - T_{5\%})/(T_{liq} - T_{5\%})$
where T_{liq} is the liquidus temperature of MIX1G and $T_{5\%}$ is the temperature at which the melt fraction of MIX1G is equal to 5%. $T_{5\%}$ and T_{liq} are assumed to be linear functions of pressure:

$T_{5\%} = c + d \cdot P$ and $T_{liq} = e + f \cdot P$, with c = 1196, d = 86.7, e = 1343, and f =73.6 (temperatures are in °C, and pressures in GPa).

Fit parameters a to f were optimized via a least squares scheme, using the experimental data of Hirschmann et al. (2003) and Kogiso et al. (2003) at 2.5 and 5 GPa, respectively, and the following constraints on $T_{5\%}$ and T_{liq}: (i) Lambart et al.'s parameterization (2011) gives $T_{5\%}$ of MIX1G equal to 1393 ± 19°C (1σ) and 1648°C± 19°C (1σ) at 2.5 and 5 GPa, respectively. (ii) T_{liq} is between 1700 and 1750°C at 5 GPa. At 2.5 GPa, the liquidus was not reached but extrapolation of the *F* vs. *T* trend allows us to localize the liquidus between 1500 and 1550°C.

Appendix 4: Potential role of CO_2

As discussed in section 2.2.3, the addition of CO_2 to the bulk composition significantly modifies melt compositions and especially, decreases their SiO_2 contents (Dasgupta et al., 2007; Herzberg and Asimow, 2008; Hirose, 1997). Based on the study of pyroxenite xenoliths carried by the Salt Lake Crater nephelinites of the Koolau Shield (Oahu island, Hawaii), Frezzotti et al. (1992) suggested that the mantle below Oahu has been metasomatized by solute-rich CO_2 fluids. Yaxley and Brey (2004) and Dasgupta et

al. (2006) proposed that carbonatitic melts produced by low melting degrees of carbonated pyroxenites can act as very efficient metasomatic agents. The capacity of carbonatitic melts to infiltrate the surrounding mantle at a very fast rate was demonstrated experimentally by Hammouda and Laporte (2000). Melting of a mantle metasomatized by carbonate-rich melts could produce low-degree melts enriched in FeO and incompatible elements (Na_2O and TiO_2) and depleted in SiO_2 (Dasgupta et al., 2006). Such a scenario was proposed by Maaløe et al. (1992) for the Koloa Volcanic Suite of Kauai: the mantle source would have been infiltrated by a carbonate-rich melt with a high concentration of Sr and REEs. In order to quantify the potential role of CO_2 on the silica concentration in melt, we consider the average melt produced by peridotites at 4 GPa for T_P = 1520 - 1560°C (~ 46 wt% SiO_2, Fig. 13) and the composition of a high-MgO melilitite sampled on the Kauai island (~ 40 wt% SiO_2, Table 2). Dasgupta et al. (2007) showed that the decrease of the silica content in peridotite-derived melts is proportional to the CO_2 content in the melt. Based on previous experimental studies of peridotites ± CO_2 between 2.8 and 8 GPa, we find that for 1 wt% CO_2 in the liquid, the SiO_2 content decreases by about 0.7 wt% (Fig. S7b). This normalization allows us to estimate the CO_2 content necessary to reproduce the low SiO_2 contents of basalts, taking into account that OIB are almost completely degassed. Accordingly, to reduce the silica content of peridotite melts from 46 to 40 wt% and thus to reproduce the SiO_2 content of the considered melilitite from Kauai, the liquid should have a CO_2 content close to 8.6 wt%. CO_2 contents in the OIB source-regions are estimated between 300 and 1300 ppm (Aubaud et al., 2005; 2006; Bureau et al., 1998; Dixon et al., 1997). Considering CO_2 as a perfectly incompatible element (i.e., its bulk partition coefficient *D* equals 0), the melting degree has to be between 0.4 and 1.5 wt% to reproduce the lowest SiO_2 contents. These low values are in agreement with the average extent of melting proposed by Dasgupta et al. (2007) for melilitites (1.7 ±1.5%).

References

Adam, J., Green, T.H. and Day, R.A., 1992. An experimental study of two garnet pyroxenite xenoliths from the Bullenmerri and Gnotuk Maars of western Victoria, Australia. Contributions to Mineralogy and Petrology, 111: 505-514.

Albarède F, Provost A (1977) Petrological and geochemical mass-balance equations: an algorithm for least-square fitting and general error analysis. Computers and Geosciences 3(2):309-326.

Arculus, R.J., 1975. Melting behavior of two basanites in the range 10–35 kbar and the effect of TiO2 on the olivine–diopside reactions at high pressures. In: C.I.o.W. Yearbook (Editor), pp. 512-515.

Asimow, P.D. and Ghiorso, M.S., 1998. Algorithmic modifications extending MELTS to calculate subsolidus phase relations. American Mineralogist, 83(9-10): 1127-1132.

Aubaud, C., Pineau, F., Hékinian, R., Javoy, M., 2005. Degassing of CO_2 and H_2O in submarine lavas from the Society hotspot. Earth and Planetary Science Letters, 235, 511-527.

Aubaud, C., Pineau, F., Hékinian, R., Javoy, M., 2006. Carbon and hydrogen isotope constraints on degassing of CO_2 and H_2O in submarine lavas from the Pitcairn hotspot (South Pacific). Geophysical Research Letters, 33(L02308).

Baker, D.R. and Eggler, D.H., 1983. Fractionation paths of Atka (Aleutians) high-alumina basalts: Constraints from phase relations. Journal of Volcanology and Geothermal Research, 18: 387-404.

Baker, M.B. and Stolper, E.M., 1994. Determining the composition of high-pressure mantle melts using diamond aggregates. Geochimica et Cosmochimica Acta, 58(13): 2811-2827.

Bartels, K.S., Kinzler, R.J. and Grove, T.L., 1991. High pressure phase relations of primitive high-alumina basalts from Medicine Lake volcano, northern California. Contributions to Mineralogy and Petrology, 108: 253-270.

Bender, J.F., Hodges, F.N. and Bence, A.E., 1978. Petrogenesis of basalts from the project FAMOUS area: Experimental study from 0 to 15 kilobars. Earth and Planetary Science Letters, 41: 277-302.

Bickle, M.J., Ford, C.E. and Nisbet, E.G., 1977. The petrogenesis of peridotitic komatiites: Evidence from high-pressure melting experiments. Earth and Planetary Science Letters, 37: 97-106.

Bureau, H., Pineau, F., Métrich, N., Semet, M.P., Javoy, M., 1998. A melt and fluid inclusion study of the gas phase at Piton de la Fournaise volcano (Réunion Island). Chemical Geology, 147, 115-130.

Cohen, L.H., Ito, K. and Kennedy, G.C., 1967. Melting and Phase relations in an anhydrous basalt to 40 kilobars. American Journal of Science, 265: 475-518.

Conte, A.M., Dolfi, D., Gaeta, M., Misiti, V., Mollo, S. and Perinelli, C., 2009. Experimental constraints on evolution of leucite-basanite magma at 1 and 10^{-4} GPa: Implications for parental compositions of Roman high-potassium magmas. European Journal of Mineralogy, 21(4): 763-782.

Dalton, J.A., Presnall, D.C., 1998. The continuum of primary carbonatitic-kimberlitic melt compositions in equilibrium with lherzolite: Data from the system CaO-MgO-Al_2O_3-SiO_2-CO_2 at 6 GPa. Journal of Petrology, 39: 1953-1964.

Dasgupta, R., Hirschmann, M.M., Smith, N.D., 2007. Partial melting experiments of peridotite + CO2 at 3 GPa and genesis of alkalic ocean island basalts. Journal of Petrology, 48(11): 2093-2124.

Dasgupta, R., Hirschmann, M.M.,Stalker, K., 2006. Immiscible transition from carbonate-rich to silicate-rich melts in the 3 GPa melting interval of eclogite + CO_2 and genesis of silica-undersaturated ocean island lavas. Journal of Petrology, 47(4), 647-671.

Dixon, J.E., Clague, D.A., Wallace, P., Poreda, R., 1997. Volatiles in alkalic basalts from the North Arch volcanic field, Hawaii: extensive degassing of deep submarine-erupted alkalic series lavas. Journal of Petrology, 38, 911-939.

Eggins, S.M., 1992. Petrogenesis of Hawaiian tholeiites: 1, phase equilibria constraints. Contributions to Mineralogy and Petrology, 110: 387-397.

Elthon, D. and Scarfe, C.M., 1984. High-pressure phase equilibria of a high-magnesia basalt and the genesis of primary oceanic basalts. American Mineralogist, 69: 1-15.

Fram, M.S. and Longhi, J., 1992. Phase equilibria of dikes associated with Proterozoic anorthosite complexes. American Mineralogist, 77: 605-616.

Frezzotti, M.L., Burke, E.A.J., De Vivo, B., Stefanini, B., Villa, I.M., 1992. Mantle fluids in pyroxenite nodules from Salt Lake Crater (Oahu, Hawaii). European Journal of Mineralogy, 4(5), 1137-1153.

Fujii, T. and Bougault, H., 1983. Melting relations of a magnesian abyssal tholeiite and the origin of MORBs. Earth and Planetary Science Letters, 62: 283-295.

Ghiorso, M.S. and Sack, R.O., 1995. Chemical mass-transfer in magmatic processes IV. A revised and internally consistent thermodynamic model for the interpolation and extrapolation of liquid-solid equilibria in magmatic systems at elevated-temperatures and pressures. Contributions to Mineralogy and Petrology, 119(2-3): 197-212.

Gudfinnsson, G., Presnall, D.C., 2005. Continuous gradations among primary carbonatitic, kimberlitic, melilititic, basaltic, picritic, and komatiitic melts in equilibrium with garnet lherzolite at 3-8 GPa. Journal of Petrology, 46: 1645-1659.

Gust, D.A. and Perfit, M.R., 1987. Phase relations of a high-Mg basalt from the Aleutian Island Arc: Implications for primary island arc basalts and high-Al basalts. Contributions to Mineralogy and Petrology, 97: 7-18.

Hammouda, T., Laporte, D., 2000. Ultrafast mantle impregnation by carbonatite melts. Geology, 28(3): 283-285.Hanson, G.N., 1977. Geochemical evolution of the suboceanic mantle. Journal of the Geological Society, 134(2), 235-253.

Herzberg, C., Gazel, E., 2009. Petrological evidence for secular cooling in mantle plumes. Nature, 458(7238): 619-622.

Herzberg, C., O'Hara, M.J., 2002. Plume-associated ultramafic magmas of Phanerozoic age. Journal of Petrology, 43(10): 1857-1883.

Herzberg, C., Asimow, P.D., Arndt, N., Niu, Y., Lesher, C.M., Fitton, J.G., Cheadle, M.J., Saunders, A.D., 2007. Temperature in ambient mantle and plumes: Constraints from basalts, picrites and komatiites. Geochemistry, Geophysics, Geosystems, 8(2), doi:10.1029/2006GC001390.

Herzberg, C. and Asimow, P.D., 2008. Petrology of some oceanic island basalts: PRIMELT2.XSL software for primary magma calculation. Geochem. Geophys. Geosyst., 9(Q09001).

Hirose, K., 1997. Partial melt compositions of carbonated peridotite at 3 GPa and role of CO_2 in alkali-basalt magma generation. Geophysical Research Letters, 24(22): 2837-2840.

Hirschmann, M.M., Kogiso, T., Baker, M.B. and Stolper, E.M., 2003. Alkalic magmas generated by partial melting of garnet pyroxenite. Geology, 31(6): 481-484.

Hirschmann, M.M., Ghiorso, M.S., Davis, F.A., Gordon, S.M., Mukherjee, S., Grove, T.L., Krawczynski, M., Médard, E. and Till, C.B., 2008. Library of experimental phase relations (LEPR): A database and Web portal for experimental magmatic phase equilibria data. Geochem. Geophys. Geosyst., 9(3).

Holbig, E.S. and Grove, T.L., 2008. Mantle melting beneath the Tibetan Plateau: Experimental constraints on ultrapotassic magmatism. Journal of Geophysical Research, 113(B04210).

Irving, A.J. and Green, D.H., 2008. Phase relationships of hydrous alkalic magmas at high pressures: Production of nepheline hawaiitic to mugearitic liquids by amphibole-dominated fractional crystallization within the lithospheric mantle. Journal of Petrology, 49(4): 741-756.

Ito, K. and Kennedy, G.C., 1974. The composition of liquids formed by partial melting of eclogites at high temperatures and pressures. Journal of Geology, 82: 383-392.

Johnston, A.D., 1986. Anhydrous P-T phase relations of near-primary high-alumina basalt from the South Sandwich Islands. Contributions to Mineralogy and Petrology, 92: 368-382.

Johnston, A.D. and Draper, D.S., 1992. Near-liquidus phase relations of an anhydrous high-magnesia basalt from the Aleutian Islands: Implications for arc magma genesis and ascent. Journal of Volcanology and Geothermal Research, 52: 27-41.

Keshav, S., Gudfinnsson, G.H., Sen, G. and Fei, Y., 2004. High-pressure melting experiments on garnet clinopyroxenite and the alkalic to tholeiitic transition in ocean-island basalts. Earth and Planetary Science Letters, 223: 365-379.

Kogiso, T. and Hirschmann, M.M., 2001. Experimental study of clinopyroxenite partial melting and the origin of ultra-calcic melt inclusions. Contributions to Mineralogy and Petrology, 142: 347-360.

Kogiso, T. and Hirschmann, M.M., 2006. Partial melting experiments of bimineralic eclogite and the role of recycled mafic oceanic crust in the genesis of ocean island basalts. Earth and Planetary Science Letters, 249: 188-199.

Kogiso, T., Hirose, K. and Takahahshi, E., 1998. Melting experiments on homogeneous mixtures of peridotite and basalt: application to the genesis of ocean island basalts. Earth and Planetary Science Letters, 162: 45-61.

Kogiso, T., Hirschmann, M.M. and Frost, D.J., 2003. High-pressure partial melting of garnet pyroxenite: possible mafic lithologies in the source of ocean island basalts. Earth and Planetary Science Letters, 216(4): 603-617.

Kogiso, T., Hirschmann, M.M. and Pertermann, M., 2004. High-pressure Partial Melting of Mafic Lithologies in the Mantle. Journal of Petrology, 45(12): 2407-2422.

Kornprobst, J., 1970. Les péridotites et les pyroxénolites du massif ultrabasique des Beni Bouchera: une étude expérimentale entre 1100 et 1550°C, sous 15 à 30 kilobars de pression sèche. Contributions to Mineralogy and Petrology, 29: 290-309.

Lambart, S., Laporte, D. and Schiano, P., 2009a. An experimental study of focused magma transport and basalt–peridotite interactions beneath mid-ocean ridges: implications for the generation of primitive MORB compositions. Contributions to Mineralogy and Petrology, 157(4): 429-451.

Lambart, S., Laporte, D. and Schiano, P., 2009b. An experimental study of pyroxenite partial melts at 1 and 1.5 GPa: Implications for the major-element composition of Mid-Ocean Ridge Basalts. Earth and Planetary Science Letters, 288(1-2): 335-347.

Lambart, S., Baker, M.B., Stolper, E.M., 2011. Parameterizing near-solidus temperatures of mantle pyroxenites and eclogites. Fall Meeting, AGU, San Francisco, Calif., abstract #V32B-04, 5-9 Dec. 2011.

Lambart, S., Laporte, D., Provost, A. and Schiano, P., 2012. Fate of pyroxenite-derived melts in the peridotitic mantle: Thermodynamical and experimental constraints. Journal of Petrology, 53(3): 451-476.

Laporte, D., Toplis, M.J., Seyler, M. and Devidal, J.-L., 2004. A new experimental technique for extracting liquids from peridotite at very low degrees of melting: application to partial melting of depleted peridotite. Contributions to Mineralogy and Petrology, 146(4): 463-484.

Le Bas, M.J., 1989. Nephelinitic and basanitic rocks. Journal of Petrology, 30: 1299-1312.

Liu, T.-C., Chen, B.-S., Pan, J.-J., Chen, P.-K. and Wu, S.-Z., 1997. A preliminary report of the experimental study of two-pyroxene andesite from Kuanyinshan, Northern Taiwan. Journal of Taiwan Normal University: Mathematics, Science & Technology, 42: 53-59.

Longhi, J., 1995. Liquidus equilibria of some primary lunar and terrestrial melts in the garnet stability field. Geochimica et Cosmochimica Acta, 59(11): 2375-2386.

Maaløe, S., James, D., Smedley, P., Petersen, S., Garmann, L.B., 1992. The Koloa Volcanic Suite of Kauai, Hawaii. Journal of Petrology, 33(4), 761-784.

Médard, E., Schmidt, M.W. and Schiano, P., 2004. Liquidus surfaces of ultracalcic primitive melts. Contributions to Mineralogy and Petrology, 148: 201-215.

Moore, K.R., Wood, B.J., 1998. The transition from carbonate to silicate melts in the CaO-MgO-SiO_2-CO_2 system. Journal of Petrology 39: 1943-1951.

Norris, J.R. and Herd, C.D.K., 2006. The Yamato 980459 Liquidus at 10 to 20 Kilobars., Lunar and Planetary Science XXXVII, League City, Texas.

O'Hara, M.J., 1972. Data reduction and projection schemes for complex compositions. In: U. EaM (Editor), Progress in experimental petrology. NERC, Manchester:Edinburgh, pp. 103-126.

Parman, S.W., Grove, T.L., 2004. Harzburgite melting with and without H2O: Experimental data and predictive modeling. Journal of Geophysical Research, 109(B2), doi: 10.1029/2003jb002566.

Pertermann, M. and Hirschmann, M.M., 2003a. Partial melting experiments on a MORB-like pyroxenite between 2 and 3 GPa: Constraints on the presence of pyroxenite in basalt source regions from solidus location and melting rate. Journal of Geophysical Research, 108(B2): 2125.

Pertermann, M. and Hirschmann, M.M., 2003b. Anhydrous Partial Melting Experiments on MORB-like Eclogite: Phase Relations, Phase Compositions and Mineral–Melt Partitioning of Major Elements at 2–3 GPa. Journal of Petrology, 44(12): 2173-2201.

Pickering-Witter, J. and Johnston, A.D., 2000. The effects of variable bulk composition on the melting systematics of fertile peridotitic assemblages. Contributions to Mineralogy and Petrology, 140: 190-211.

Pilet, S., Baker, M.B. and Stolper, E.M., 2008. Metasomatized Lithosphere and the Origin of Alkaline Lavas. Science, 320: 916.

Putirka, K.D., 2008. Thermometers and Barometers for Volcanic Systems. Reviews in Mineralogy & Geochemistry, 69: 61-120.

Putirka, K.D., Johnson, M., Kinzler, R.J. and Walker, D., 1996. Thermobarometry of mafic igneous rocks based on clinopyroxene-liquid equilibria, 0-30 kbar. Contributions to Mineralogy and Petrology, 123: 92-108.

Putirka, K.D., Ryerson, F.J. and Mikaelian, H., 2003. New igneous thermobarometers for mafic and evolved lava compositions, based on clinopyroxene + liquid equilibria. American Mineralogist, 88: 1542-1554.

Ryabchikov, I.D., Brey, G., Kogarko, L.N., Bulatov, V.K., 1989. Partial melting of carbonatized peridotite at 50 kbar. Geokhimiya, 1: 3-9.

Schiano, P., Eiler, J.M., Hutcheon, I.D. and Stolper, E.M., 2000. Primitive CaO-rich, silica-undersaturated melts in island arcs: Evidence for the involvement of clinopyroxene-rich lithologies in the petrogenesis of arc magmas. Geochem. Geophys. Geosyst., 1(5).

Skjerlie, K.P. and Patiño Douce, A.E., 2002. The fluid-absent partial melting of a zoisite-bearing quartz eclogite from 1.0 to 3.2 GPa; Implications for melting in thickened continental crust and for subduction-zone processes. Journal of Petrology, 43(2): 291-314.

Sobolev, A.V., Hofmann, A.W., Kuzmin, D.V., Yaxley, G.M., Arndt, N.T., Chung, S.-L., Danyushevsky, L.V., Elliott, T., Frey, F.A., Garcia, M.O., Gurenko, A.A., Kamenetsky, V.S., Kerr, A.C., Krivolutskaya, N.A., Matvienkov, V.V., Nikogosian, I.K., Rocholl, A., Sigurdsson, I.A., Sushchevskaya, N.M. and Teklay, M., 2007. The Amount of Recycled Crust in Sources of Mantle-Derived Melts. Science, 316(5823): 412-417.

Spandler, C., Yaxley, G., Green, D.H. and Rosenthal, A., 2008. Phase Relations and Melting of Anhydrous K-bearing Eclogite from 1200 to 1600°C and 3 to 5 GPa. Journal of Petrology, 49(4): 771-795.

Takahashi, E., Nakajima, K. and Wright, T.L., 1998. Origin of the Columbia River basalts: melting model of a heterogeneous plume head. Earth and Planetary Science Letters, 162: 63-80.

Thompson, R.N., 1974. Primary Basalts and magma genesis I. Skye, North-West Scotland. Contributions to Mineralogy and Petrology, 45: 317-341.

Thompson, R.N., 1975. Primary Basalts and Magma Genesis II. Snake River Plain, Idaho, U.S.A. Contributions to Mineralogy and Petrology, 52: 213-232.

Tsuruta, K. and Takahashi, E., 1998. Melting study of an alkali basalt JB-1 up to 12.5 GPa: behavior of potassium in the deep mantle. Physics of the Earth and Planetary Interiors, 107: 119-130.

Tuff, J., Takahahshi, E. and Gibson, S.A., 2005. Experimental constraints on the role of garnet pyroxenite in the genesis of high-Fe mantle plume derived melts. Journal of Petrology, 46(10): 2023-2058.

Villiger, S., Ulmer, G.C., Müntener, O. and Thompson, A.B., 2004. The liquid line of descent of anhydrous, mantle-derived, tholeiitic liquids by fractional and equilibrium crystallization - An experimental study at 1.0 GPa. Journal of Petrology, 45(12): 2368-2388.

Walter, M.J., 1998. Melting of garnet peridotite and the origin of komatiite and depleted lithosphere. Journal of Petrology, 39(1): 29-60.

Wagner, T.P. and Grove, T.L., 1998. Melt/harzburgite reaction in the petrogenesis of tholeiitic magma from Kilauea volcano, Hawaii. Contributions to Mineralogy and Petrology, 131: 1-12.

Wasylenki, L.E., Baker, M.B., Kent, A.J.R. and Stolper, E.M., 2003. Near-solidus melting of the shallow upper mantle: Partial melting experiments on depleted peridotite. Journal of Petrology, 44(7): 1163-1191.

Yasuda, A., Fujii, T. and Kurita, K., 1994. Melting phase relations of an anhydrous mid-ocean ridge basalt from 3 to 20 GPa: Implications for the behavior of subducted oceanic crust in the mantle. Journal of Geophysical Research, 99(B5): 9401-9414.

Yaxley, G. M., Brey, G.P., 2004. Phase relations of carbonate-bearing eclogite assemblages from 2.5 to 5.5 GPa: implications for petrogenesis of carbonatites. Contributions to Mineralogy and Petrology, 146, 606-619.

Yaxley, G. and Green, D.H., 1998. Reactions between eclogite and peridotite : mantle refertilisation by subduction of oceanic crust. Schweizerische mineralogische und petrographische Mitteilungen, 78: 243-255.

Yaxley, G.M., Sobolev, A.V., 2007. High-pressure partial melting of gabbro and its role in the Hawaiian magma source. Contributions to Mineralogy and Petrology, 154: 371-383.

Yoder, H.S. and Tilley, C.E., 1962. Origin of basalt magmas: An experimental study of natural and synthetic rock systems. Journal of Petrology, 3(3): 342-532.

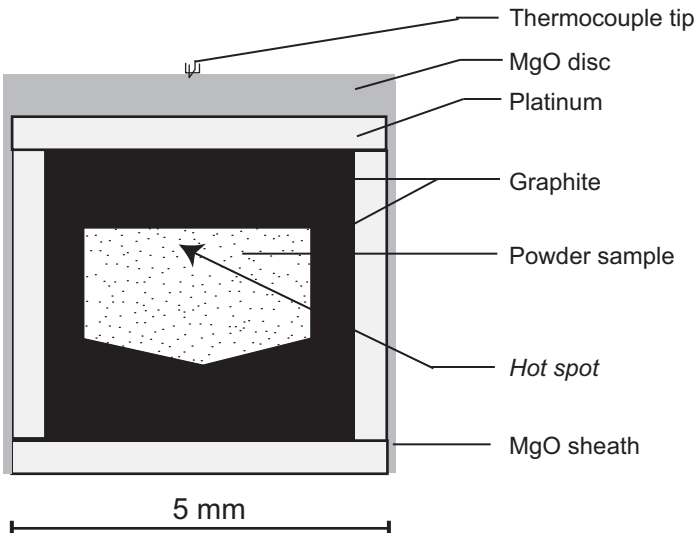

Fig. S1 Scaled sketch of the container geometry.

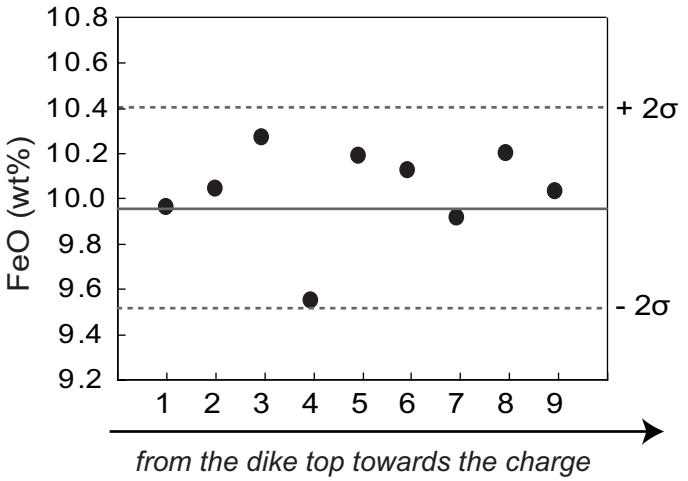

Fig. S2 FeO contents of melt at various positions in the microdikes of #40-H3 (referred by numbers in **Fig. 6b**) compared to the mean FeO content of melt (solid grey line; 9.96 wt%). The mean content has been determined from 13 analyses made in three dikes: the two dykes in **Fig. 6b** at the top of the sample, a third one at the bottom.

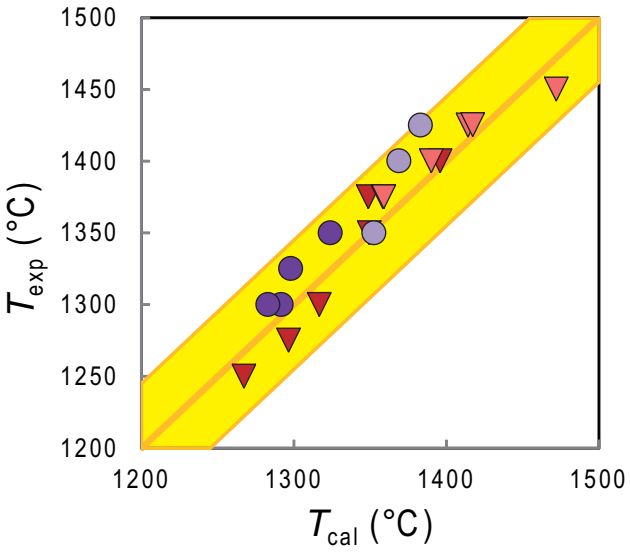

Fig. S3 Comparison between experimental temperatures, T_{exp}, and temperatures calculated using the Cpx-liquid geothermometer of Putirka et al. (1996, 2003), T_{cal}. M5-40 experiments are represented by triangles and M7-16 experiments by circles. Dark and light colors represent experiments performed at 2 and 2.5 GPa, respectively. The yellow area indicates the geothermometer uncertainty (± 45°C).

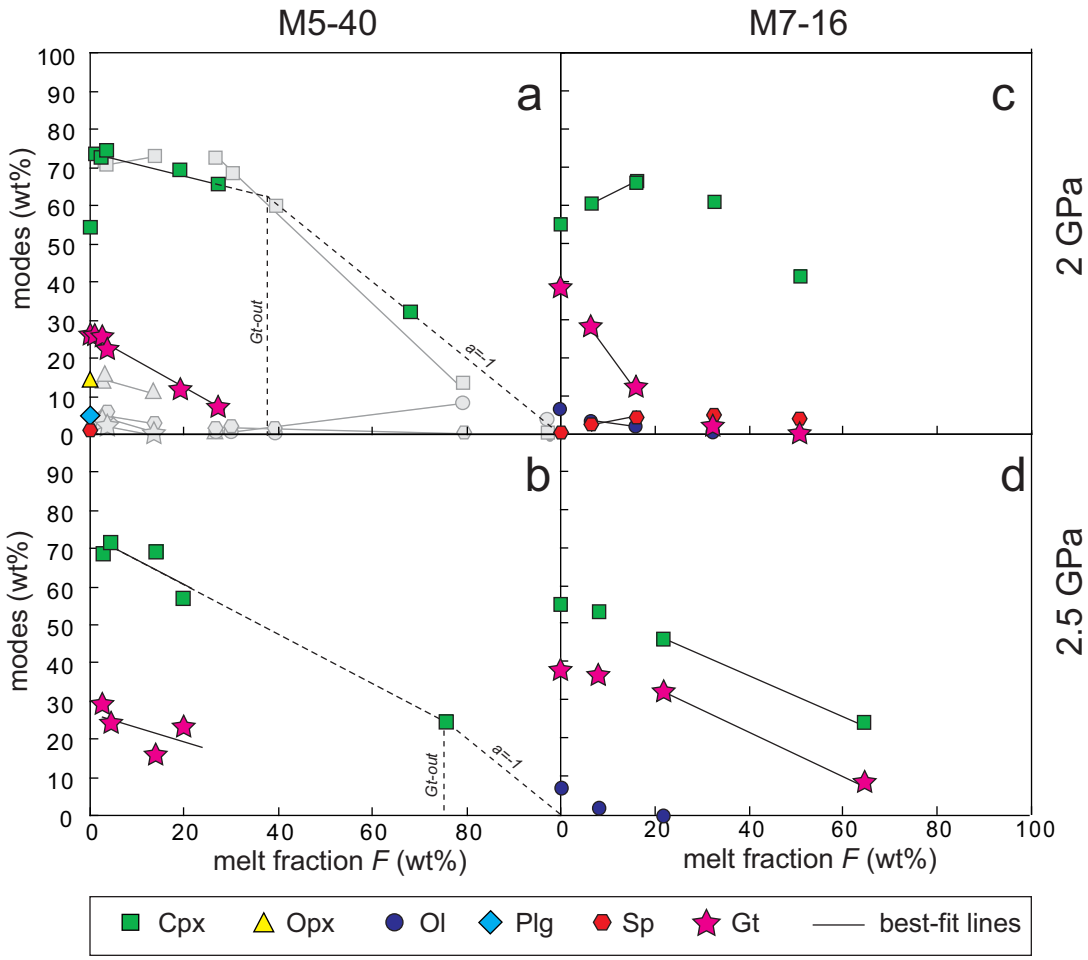

Fig. S4 Fractions (wt%) of solid phases *vs* melt fraction *F* for pyroxenites **(a-b)** M5–40 and **(c-d)** M7–16 at 2 and 2.5 GPa. The *straight lines* are the best-fit lines used to compute the coefficients of the melting reactions. Symbols are given in the inset. The uncertainties on phase percentages are given in Table 1. *Grey symbols* in **(a)** are fractions of solid phases for M5-40 at 1.5 GPa. The *dashed lines* in **(a)** and **(b)** are used to estimate the melt fraction at which Gt is consumed (see Appendix A1.5).

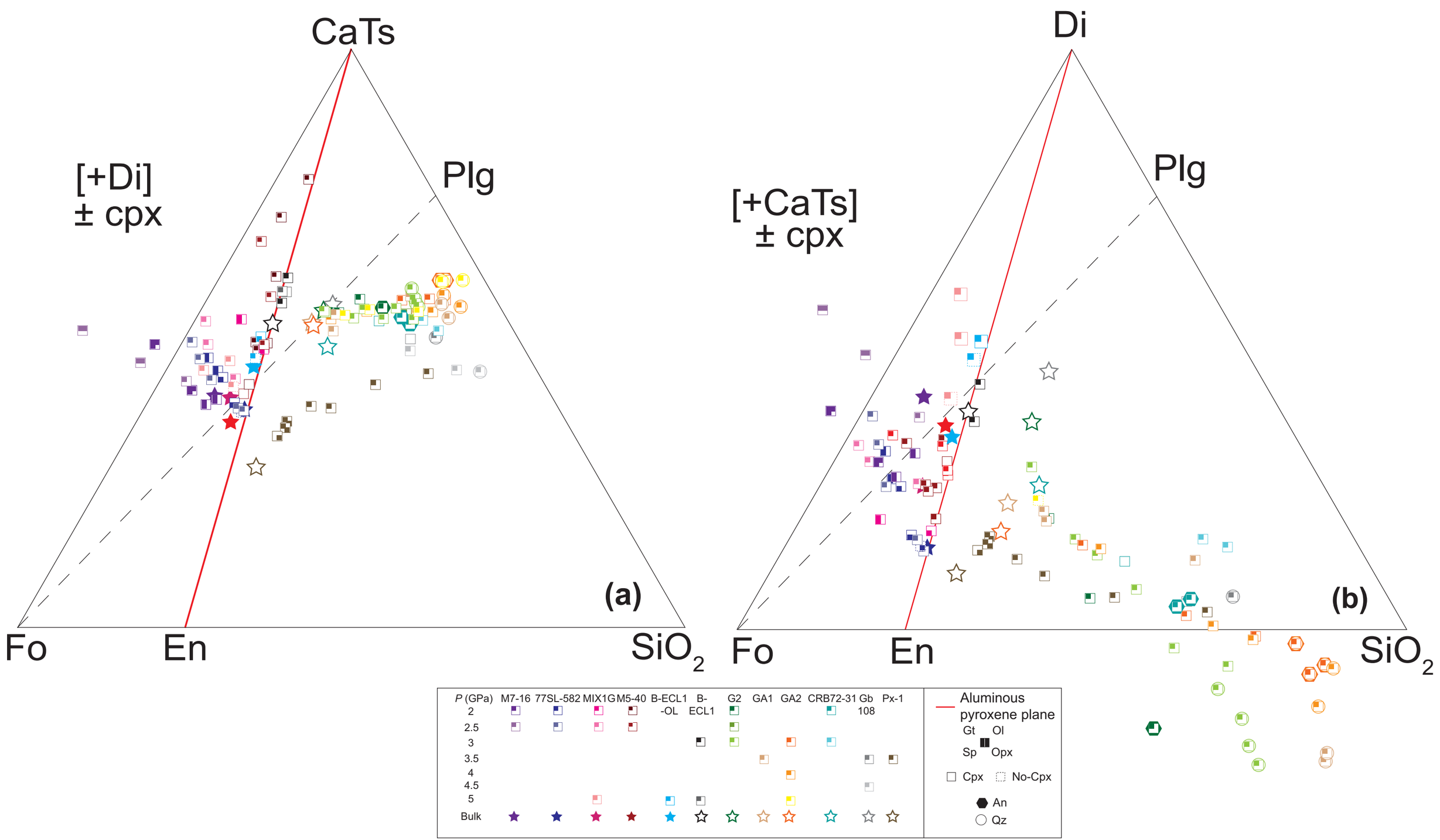

Fig. S5 Phase assemblages and melt compositions in partial melting experiments of pyroxenites between 2 and 5 GPa; melts are projected from Di **(a)** and from CaTs **(b)**, using the method of O'Hara (1972). Present phases are indicated by filled split squares for Gt, Sp, Ol and Opx. Almost all experiments are saturated with Cpx. Assemblages without Cpx are represented with dashed squares. Symbols of other phases are as in the inset. References are: M7-16 and M5-40, this study and Lambart et al. (2012); MIX1G, Hirschmann et al. (2003) and Kogiso et al. (2003); 77SL-582, Keshav et al. (2004); B-ECL1 and B-ECL1-OL, Kogiso et Hirschmann (2006); G2, Pertermann and Hirschmann (2003b); GA1, Yaxley et Green (1998); GA2, Spandler et al. (2008); CRB72-31, Takahashi at al. (1998); Gb108, Yaxley and Sobolev (2007); Px-1, Sobolev et al. (2007). Abbreviations as in **Fig. 3**.

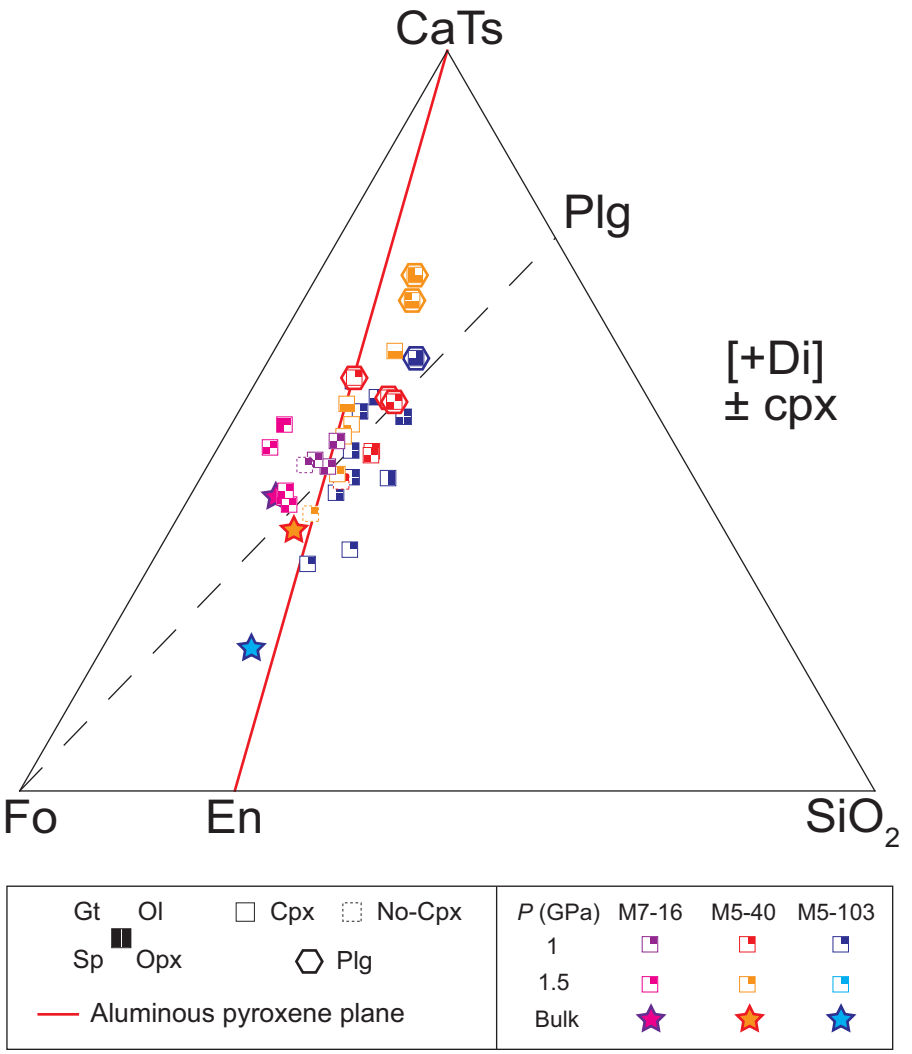

Fig. S6 Phase assemblages and melt compositions in partial melting experiments of pyroxenites at 1 and 1.5 GPa (Lambart et al., 2009); melts are projected from Di, using the method of O'Hara (1972). Symbol of present phases are as in the inset.

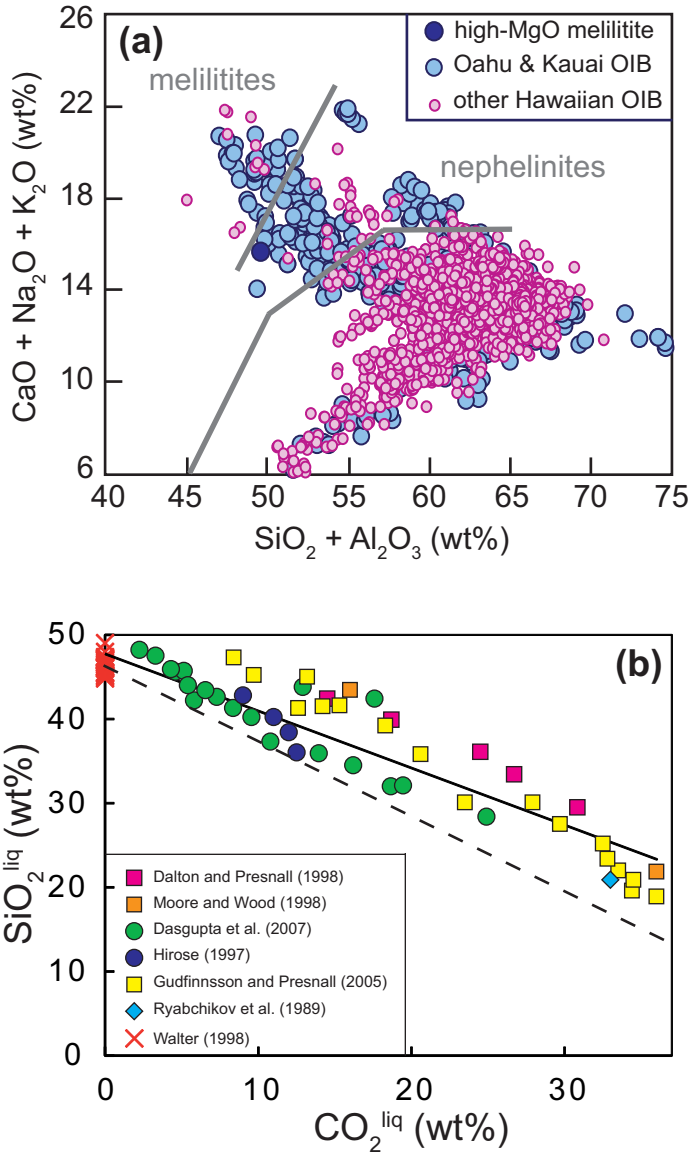

Fig. S7 (a) Classification of highly alkalic lavas as melilitites and nephelinites, following the scheme of Le Bas (1989), applied to hawaiian island basalts (GEOROC database: http://georoc.mpch-mainz.gwdg.de/georoc/). The dark blue circle represents composition of the high-MgO melilitite reported in Table 2. **(b)** Measured concentrations of SiO_2 vs. estimated concentrations of CO_2 in carbonated silicate melts from partial melting experiments of simple and complex peridotite ± CO_2 between 2.8 and 8 GPa. SiO_2 contents are normalized on a CO_2-free basis. The linear fit (solid line) of the melt compositions between 0 and 37 wt% CO_2 in the melt is given by SiO_2^{liq} = 47.7 - 0.68 CO_2^{liq} and is compared with the fit obtain by Dasgupta et al. (2007) with the non normalized SiO_2 contents (SiO_2^{liq} = 46.2 - 0.89 CO_2^{liq}, dashed line).

Table S1. Compositions of starting materials used in experimental studies of pyroxenite partial melting (listed in chronological order)

Reference	Purpose of experiments[a]	P[b] (GPa)	Starting material	SD/SE[c]	SiO_2	TiO_2	Al_2O_3	Cr_2O_3	FeO^T	MnO	MgO	CaO	Na_2O	K_2O	P_2O_5	Mg#	F_{min}[d]
Yoder and Tilley (1962)	PM – liq, mnl	0 - 3.14	35090	SE	50.05	1.55	13.37	-	13.73	0.25	6.49	11.00	2.38	0.36	0.12	45.7	
Cohen et al. (1967)	PM – mnl	0 - 4	NM5	SE	49.93	1.34	16.75	-	11.40	0.18	7.59	9.33	2.92	0.37	0.18	54.3	
Kornprobst (1970)	PR	1.5 - 3	M7-58	SD	44.26	0.58	10.91	0.19	10.19	0.15	16.75	12.15	1.19	0.04	0.10	74.6	
			M7-703	SD	46.21	0.69	12.49	0.23	10.10	0.16	13.63	13.87	1.88	0.03	0.18	70.6	
			M5-43	SD	44.82	0.67	15.38	0.25	10.99	0.20	11.31	14.41	1.34	0.09	0.10	64.7	
			M5-367	SD	43.48	1.10	15.19	0.11	16.22	0.48	11.24	10.57	1.00	0.13	0.10	55.3	
Ito and Kennedy (1974)	PM – liq	0 - 3.5	eclogite	SD	46.46	0.40	16.43	-	12.1	0.33	14.20	7.98	1.89	0.09	-	67.7	
Thompson (1974)	PR – liq, mnl	0.8 - 3.1	66018	SD	46.12	1.81	13.94	-	12.22	0.18	11.08	9.05	3.11	0.57	0.23	61.8	
		0.5 - 2.6	SK 971	SE	46.94	1.37	17.15	-	11.73	0.19	7.69	9.73	3.01	0.43	0.18	59.7	
		1 - 2.2	SK 931	SE	46.86	3.34	15.68	-	13.28	0.20	4.31	6.66	4.75	0.77	0.47	36.7	
Arculus (1975)	PM – liq	1 - 3	AJI2164	SD	44.17	2.75	13.26	0.03	11.33	0.18	10.30	8.77	3.71	2.02	0.97	61.8	
		1 - 3.5	G531	SD	44.78	1.02	15.95	0.03	9.13	0.18	10.71	12.81	2.38	0.91	0.37	67.6	
Thompson (1975)	PR – liq, mnl	0.5 - 3.5	59-P-13	SE	47.76	3.03	14.93	-	13.59	0.20	6.70	9.41	2.62	0.75	0.53	46.8	
			OB 32	SE	47.17	4.15	13.34	-	15.22	0.23	4.42	7.68	3.40	2.00	1.39	34.1	
Bickle et al. (1977)	PR	1 - 4	NG 157	SD	47.59	0.29	6.34	0.42	10.79	0.17	28.18	5.91	0.16	0.44	0.02	82.3	
			NG 152	SD	46.90	0.22	5.08	0.44	10.62	0.14	31.81	5.05	0.02	0.03	0.01	84.2	
			NG 7638	SD	47.96	0.36	7.44	0.41	11.39	0.20	24.35	7.46	0.64	0.06	0.03	79.2	
			NG 7621	SD	48.76	0.42	8.44	0.43	12.09	0.19	20.45	8.58	0.39	0.50	0.04	75.1	
Bender et al. (1978)	PR – mode, liq, mnl	0 - 1.5	527-1-1	SE	48.2	0.73	16.3	0.05	-	0.25	10.7	12.0	1.95	0.09	-	-	57.3
Baker and Eggler (1983)	PR – liq, mnl	0 - 2	AT-1	SE	49.89	1.02	19.43	-	9.45	0.28	4.79	9.17	3.39	0.76	-	47.5	
Fujii and Bougault (1983)	PR – liq, mnl	0, 0.75 - 1.5	ARP 74 10-16	SE	50.0	0.86	15.5	-	8.05	0.17	10.5	12.2	2.10	0.13	0.14	59.9	
Elthon and Scarfe (1984)	PR – liq, mnl	1 - 2	NT-23	SD	47.25	0.79	13.64	-	9.77	0.14	17.61	9.58	0.89	0.06	-	76.3	
Johnston (1986)	PR – mode, liq, mnl	1 - 3.1	SSS.1.4	SE	50.26	0.54	18.46	-	7.61	0.21	7.32	11.81	1.80	0.25	-	63	27
Gust and Perfit (1987)	PR – liq	0, 0.5 - 2	MK-15	SE	51.20	0.75	15.69	-	9.21	0.16	9.64	10.21	2.77	0.92	0.21	67.4	
Bartels et al. (1991)	PR – mode, liq, mnl	1 - 1.5	79-35g	SE	47.7	0.65	18.6	-	8.53	0.15	9.92	12.1	2.25	0.07	0.05	67.5	11
		0, 1 - 1.2	82-72f	SE	47.7	0.59	18.5	-	8.20	0.15	10.5	12.0	2.16	0.07	0.06	69.5	37
Adam et al. (1992)	PR – mnl	0.6 - 3	DR9734	SD	46.82	0.23	15.00	0.08	7.34	0.0	12.34	16.80	1.36	0.03	-	75.0	
			DR10165	SD	46.21	0.39	13.70	0.41	7.26	0.14	20.10	11.34	0.45	0.0	-	83.1	
Eggins (1992)	PR	2	K-iki	SD	47.76	2.09	10.53	0.13	11.61	0.15	15.98	9.26	1.79	0.43	0.20	71.0	
Fram and Longhi (1992)	PR – liq, mnl	0 - 3	500B	SE	55.85	0.52	22.92	0.01	3.50	0.06	1.40	9.55	4.67	0.90	0.16	41.6	
		0 - 1.5	HLCA	SE	50.02	1.85	17.51	0.03	10.97	0.15	6.67	8.78	2.93	0.44	0.16	52.0	
Johnston and Draper (1992)	PR	0 - 2	ID-16	SE	49.3	0.6	15.8	-	8.8	0.16	11.4	10.7	2.10	0.51	0.10	70	
Yasuda et al. (1994)	PM – liq, mnl	3 - 20	NAM-7	SE	49.71	1.71	15.68	-	9.37	0.18	8.43	11.73	2.76	0.23	0.02	61.6	
Longhi (1995)	PR – mode, liq, mnl	2.8 - 3	TB492	SD	43.3	1.84	6.47	0.61	22.0	0.23	21.9	3.27	0.3	0.06	-	64.0	51.5

Reference	Purpose of experiments[a]	P[b] (GPa)	Starting material	SD/SE[c]	SiO_2	TiO_2	Al_2O_3	Cr_2O_3	FeO^T	MnO	MgO	CaO	Na_2O	K_2O	P_2O_5	Mg#	F_{min}[d]
			TB992	SD	42.24	2.15	7.58	0.70	21.31	0.33	20.11	5.26	0.29	0.03	-	62.7	28.1
			TB1292	SD	44.8	1.87	6.75	0.69	18.6	0.29	22.1	3.56	0.28	0.03	-	67.9	63.2
			TB393	SD	40.2	2.17	8.23	0.65	20.3	0.25	22.6	5.24	0.4	0.04	-	66.5	56.5
			TB593	SD	41.2	1.95	9	0.67	19.6	0.23	21.8	5.6	0.33	0.04	-	66.5	22.4
			TB693	SD	46.4	1.73	6.2	0.59	15.9	0.34	19.9	8.83	0.91	0.04	-	69.1	40.4
			RD794	SD	42.6	0.27	13.5	0.74	8.75	0.03	25.5	7.22	1.14	0.06	0.04	83.9	37.2
			RD893	SD	45.4	0.21	11.6	0.70	8.54	0.04	26.8	6.2	1.21	0.06	0.05	84.8	48.7
			RD1093	SD	44.58	0.24	12.17	0.66	8.51	0.03	26.09	6.44	1.20	0.04	0.05	84.5	37.0
Liu et al. (1997)	PR	0, 1 - 2	2px-And	SE	56.93	0.67	18.42	-	6.03	0.13	5.43	7.57	3.01	1.81	-	61.6	
Takahashi et al. (1998)	PM – liq, mnl	0 - 3	CRB72-151	SE	53.80	1.13	15.19	-	9.40	0.16	6.12	10.09	2.88	0.69	0.26	53.7	
			CBR75-219	SE	51.52	1.70	14.98	-	11.83	0.18	5.96	9.71	2.76	0.60	0.32	47.3	
			CRB72-180	SE	49.17	3.15	14.45	-	13.91	0.19	5.70	8.94	2.54	1.01	0.65	42.2	
			CRB72-31	SE	50.76	1.48	16.02	-	9.52	0.14	8.23	10.77	2.29	0.39	0.19	60.6	
Tsuruta and Takahashi (1998)	PM – liq, mnl	0 - 12.5	JB-1	SE	53.25	1.37	14.83	0.05	8.36	0.17	7.89	9.48	2.85	1.46	0.26	62.7	
Wagner and Grove (1998)	PM – mode, liq, mnl	1 - 2.2	Prim K-thol	SD	48.8	1.77	10.3	-	11.6	0.17	17.2	8.25	1.52	0.27	0.16	72.6	35
Yaxley and Green (1998)	PM – mode, liq, mnl	3.5	GA1	SE	50.35	1.49	16.53	0.0	9.83	0.17	7.94	9.60	3.49	0.44	0.16	59.0	13.2
Kogiso and Hirschmann (2001)	PM – mode, liq, mnl	1	Pyrox2B	SD	51.6	0.54	5.58	-	7.0	0.10	16.2	18.2	0.84	-	-	80.5	6
Kogiso and Hirschmann (2001)	PM – mode, liq, mnl	1, 2	OLCPX1	SD	47.9	0.47	4.49	-	9.26	0.13	23.4	13.72	0.63	-	-	81.8	5
		1	OLCPX2	SD	48.7	0.39	4.13		7.9	0.12	24.4	13.7	0.57	-	-	84.6	13
Skjerlie and Patiño Douce (2002)	PM – liq, mnl	1 - 3.2	Verpenesset ecl.	SE	49.96	0.76	19.97	-	5.83	0.11	8.15	12.72	2.57	0.14	-	71.4	
Hirschmann et al. (2003) ; Kogiso et al. (2003)	PM – mode, liq, mnl	2 – 7.5	MIX1G	SD	45.6	0.90	15.2	0.11	7.8	0.15	16.67	11.48	1.4	0.04	0.01	79.3	14
Pertermann and Hirschmann (2003a; 2003b)	PM – mode, liq, mnl	2 - 3	G2	SE	50.1	1.97	15.8	-	9.4	0.17	7.9	11.7	3.0	0.03	-	60.1	2
			G2K	SE	50.8	1.90	15.22	-	9.0	0.16	7.91	11.68	3.02	0.26		61.0	14.3
Keshav et al. (2004)	PM – mode, liq, mnl	2, 2.5	77SL-582	SD	46.4	0.63	16.42	0.14	7.6	0.22	16.5	10.74	0.99	-	-	79.4	18.1
Médard et al. (2004)	PR – mode, liq, mnl	0.7 - 1.5	CaHy	SE	49.65	0.40	11.18	-	7.59	-	14.53	15.25	1.12	0.28	-	77.3	60
Villiger et al. (2004)	PR – mode, liq, mnl	1	HK#19	SE	49.10	0.60	15.17	0.36	7.54	0.14	13.10	12.27	1.58	0.08	-	76	72.6
			HK#19.2	SE	48.67	0.57	14.55	0.34	7.56	0.14	14.81	11.73	1.50	0.08	-	78	98.1
			fr1	SE	49.78	0.59	14.32	0.36	7.43	0.15	14.02	11.69	1.58	0.08	-	77	90.1
			fr2	SE	50.47	0.60	14.78	0.25	7.25	0.16	12.38	12.30	1.73	0.09	-	75	75.1
Tuff et al. (2005)	PR – mode, liq, mnl	0 - 7	97SB68	SD	46.91	1.75	9.09	-	14.90	0.17	14.94	8.08	1.94	0.68	0.19	64	5
Kogiso and Hirschmann (2006)	PM – mode, liq, mnl	3, 5	B-ECL1	SD-SE	46.0	1.7	15.7	0.04	10.6	0.21	10.1	12.5	2.5	0.04	-	62.9	28
			B-ECL1-OL	SD	46.7	1.5	13.6	0.03	12.4	0.19	11.6	11.4	2.24	0.04	-	62.4	60

Reference	Purpose of experiments[a]	P[b] (GPa)	Starting material	SD/SE[c]	SiO_2	TiO_2	Al_2O_3	Cr_2O_3	FeO^T	MnO	MgO	CaO	Na_2O	K_2O	P_2O_5	Mg#	F_{min}[d]
Norris and Herd (2006)	PR	1 - 2	Y980459	SD	46.89	0.53	5.37	0.54	17.96	0.48	19.76	6.28	0.5	0.01	0.26	66.2	
Sobolev et al. (2007)	PM – mode, liq	3.5	Px-1	SE	52.67	0.64	11.26	0.25	7.55	0.12	18.48	7.05	1.52	0.06	-	81.4	8
Yaxley and Sobolev (2007)	PM –liq, mnl	3.5, 4.5	Gb 108	SE	52.04	0.42	16.68	-	5.96	-	8.93	12.36	3.26	0.04	-	72.8	
Holbig and Grove (2008)	PM – mode, liq, mnl	1 - 2.2	Bb-107	SD	45.42	1.26	12.55	-	9.02	0.16	10.42	12.24	3.35	3.94	1.55	67.3	32
Irving and Green (2008)	PM – liq, mnl	0 - 3.1	2102	SD	49.10	2.17	15.40	0.04	10.0	0.18	7.10	6.30	5.60	2.90	0.68	55.9	
Pilet et al. (2008)	PM – mode, liq	1.5	AG4	SD	39.1	5.39	14.07	-	9.8	0.18	11.92	12.06	2.57	1.18	0.44	66.0	25
			AG7	SD	44.1	3.63	11.37	-	6.9	0.13	12.63	17.01	1.70	0.80	0.06	76.5	37
			Free H_2O - AG4	SD	39.9	5.49	14.2	-	11.1	0.20	12.1	12.5	2.42	1.1	0.43	66.0	46
Spandler et al. (2008)	PM – mode, liq, mnl	3 - 5	GA2	SE	49.68	1.82	16.94	0.08	9.71	0.09	8.08	9.28	3.34	0.37	0.23	59.7	4
Conte et al. (2009)	PR – mode, liq, mnl	0, 1	MF	SD	47.06	0.67	12.04	0.09	7.54	0.14	12.76	13.70	1.22	3.30	0.28	75.1	39.4
Lambart et al. (2009b)	PM – mode, liq	1 – 1.5	M5-103	SD	51.64	0.09	7.17	0.60	4.97	0.10	24.57	10.13	0.71	0.02	-	89.8	2.6
Lambart et al. (2009b, 2012, this study)	PM – mode, liq	1 - 2.5	M5-40	SD	48.53	0.52	12.37	0.12	9.02	0.2	16.64	10.89	1.65	0.06	-	76.7	1.1
			M7-16	SD	43.58	0.75	13.73	0.07	14.51	0.30	12.52	13.77	0.75	0.03	-	60.6	2.9

Total iron given as FeO.

[a] Purpose of experiments and parameters determined in the run products. Purpose: Partial melting study ("PM") or phase relations ("PR"). Parameters: phase proportions ("mode"), liquid ("liq") and/or mineral ("mnl") compositions.

[b] Pressure range of experiments; '0' is 0.1 MPa.

[c] Type of pyroxenites: silica-deficient (SD) or silica-excess (SE) pyroxenite (Kogiso et al., 2004; Schiano et al., 2000).

[d] F_{min}: minimum degree of melting studied.

Table S2. Compositions (mol%) of melts from basalt – peridotite mixes KG1[a], KG2[a] and W3[b] (L_{KG1}, L_{KG2} and L_W), and from peridotites HK66[c] and PHN 1611[d], (L_{HK} and L_{PHN}) in equilibrium with Ol – Opx – Cpx – Sp at 2 GPa.

	L_{KG1}	L_{KG2}	L_W	L_{HK}	L_{PHN}
F[e]	8	4		-	6.4
SiO_2	50.3	52.4	45.06	48.9	49.4
TiO_2	2.0	1.5	0.80	1.1	1.5
Al_2O_3	11.2	12.0	9.30	9.7	10.0
Cr_2O_3	0.02	0.02	0.02	0.05	0.04
FeO[f]	9.1	7.2	9.42	9.0	8.0
MnO	-	-	0.05	0.25	0.17
MgO	13.4	12.7	20.59	16.7	16.2
CaO	6.4	6.3	12.20	10.2	10.7
Na_2O	6.4	6.1	2.18	3.91	2.51
K_2O	1.1	1.8	0.05	0.28	1.45
Mg#[g]	59.6	63.9	68.6	65.1	66.8

[a] Kogiso et al. (1998); [b] Parman and Grove (2004); [c] Hirose and Kushiro (1993); [d] Kushiro (1996); [e] *F*: melt fraction (wt%); [f] FeO: total FeO; [g] Mg#: molar ratio 100 × MgO/(MgO+FeO)

Table S3. Major-element compositions and potential temperatures[a] (T_P) of px-MORB.

Sample	Location	SiO_2	TiO_2	Al_2O_3	FeO^T	MgO	CaO	Na_2O	K_2O	T_P
1559-1647	near East Pacific Ridge (EPR)	48.57	1.02	17.45	8.59	9.31	12.60	2.42	0.04	1426
1564-1949	seamount	48.58	0.94	16.93	9.11	9.25	12.89	2.26	0.04	1459
R60-1		48.47	1.24	17.69	8.57	9.15	11.92	2.88	0.09	1422
VG3075	Kane Fracture zone	48.20	0.93	17.94	9.46	9.04	11.87	2.52	0.04	1479
VG3079		48.23	0.92	18.13	9.38	9.13	11.55	2.59	0.06	1475
18-1-1		47.73	1.05	17.82	9.33	9.21	12.27	2.57	0.03	1464
VG9793	Central Lau spreading-	48.14	1.07	17.70	9.08	9.17	12.30	2.52	0.02	1454
VG9794	center	47.84	1.04	17.78	9.24	9.28	12.27	2.53	0.02	1459
VG9795		47.50	1.05	17.87	9.39	9.27	12.32	2.58	0.03	1464
VG8251	EPR spreading-center	47.53	1.20	17.67	10.27	9.01	11.88	2.38	0.06	1517
VG8253		47.78	1.21	17.64	10.12	9.18	11.59	2.43	0.07	1511
VG8254		47.87	1.21	17.50	10.23	9.13	11.62	2.37	0.07	1518
VG8256		47.74	1.08	17.50	10.23	9.50	11.59	2.31	0.04	1516
K10-2	Galapagos spreading-center	48.58	0.84	17.53	9.02	9.23	12.68	2.08	0.04	1458
K10-3		48.52	0.87	17.64	9.06	9.07	12.68	2.11	0.05	1461
K10-5		48.51	0.87	17.69	9.00	9.07	12.74	2.09	0.04	1457
K10-7		48.54	0.84	17.63	9.08	9.10	12.67	2.11	0.04	1462
K10-9		48.47	0.87	17.65	9.15	9.16	12.57	2.08	0.04	1466
K10-13		48.25	1.02	17.37	9.51	9.17	12.34	2.30	0.04	1482
K10-17		48.67	0.82	17.70	9.01	9.28	12.40	2.07	0.05	1459
K10-20		48.65	0.84	17.62	9.04	9.27	12.43	2.09	0.05	1461
10-30		48.62	0.84	17.62	9.02	9.32	12.44	2.10	0.04	1459
K10-33		48.62	0.84	17.49	9.08	9.51	12.39	2.04	0.04	1462
10-34		48.41	1.00	17.46	9.56	9.06	12.11	2.37	0.05	1487
K10-35		48.65	0.81	17.40	9.01	9.61	12.43	2.05	0.04	1457
K10-36		48.63	0.82	17.49	9.11	9.47	12.36	2.07	0.04	1464
20-1		48.67	0.97	17.15	9.66	9.00	12.22	2.29	0.04	1497
VG9224	Mid-Atlantic Ridge (MAR)	48.03	0.80	17.82	9.56	9.11	12.13	2.36	0.01	1484
VG9225	spreading-center	48.01	0.81	17.87	9.51	9.10	12.14	2.39	0.02	1481
VG9226		48.04	0.77	17.85	9.60	9.05	12.13	2.38	0.01	1487
VG9227		48.01	0.82	17.91	9.40	9.06	12.22	2.39	0.02	1475
VG9228		48.02	0.80	17.84	9.55	9.07	12.14	2.38	0.01	1484
VG9229		47.81	0.79	17.83	9.67	9.19	12.14	2.38	0.01	1487
VG9230		47.86	0.81	17.87	9.68	9.11	12.12	2.37	0.01	1488
VG9231		47.88	0.77	17.75	9.88	9.22	11.99	2.32	0.01	1500
VG9232		47.89	0.80	17.83	9.63	9.21	12.06	2.36	0.01	1486
VG9233		48.09	0.80	17.75	9.54	9.09	12.15	2.40	0.01	1483y
VG9234		47.97	0.79	17.81	9.66	9.12	12.10	2.38	0.01	1488
VG9236		47.96	0.78	17.81	9.57	9.16	12.15	2.36	0.01	1484
VG9237		47.97	0.78	17.84	9.62	9.23	12.02	2.35	0.01	1487
VG9238		48.09	0.79	17.78	9.53	9.15	12.08	2.38	0.01	1483
VG9240		48.25	0.81	17.79	9.47	9.04	12.09	2.38	0.01	1482
VG9242		47.89	0.77	17.75	9.82	9.19	12.02	2.37	0.01	1496
VG9243		47.98	0.79	17.80	9.70	9.06	12.07	2.39	0.01	1491
VG9244		48.15	0.81	17.89	9.41	9.05	12.15	2.36	0.01	1478
VG9245		48.06	0.78	17.83	9.47	9.15	12.16	2.36	0.01	1479
VG9246		47.99	0.77	17.72	9.79	9.09	12.08	2.38	0.01	1496
VG9247		47.94	0.80	17.79	9.82	9.03	12.05	2.36	0.01	1498
VG9248		48.03	0.80	17.72	9.70	9.13	12.04	2.37	0.01	1492
VG9251		47.86	0.77	17.77	9.70	9.11	12.20	2.38	0.02	1489

Sample	Location	SiO_2	TiO_2	Al_2O_3	FeO^T	MgO	CaO	Na_2O	K_2O	T_P
VG9252	MAR spreading-center	47.93	0.78	17.76	9.68	9.15	12.16	2.38	0.01	1489
VG9257		47.96	0.81	17.76	9.60	9.16	12.18	2.36	0.01	1485
VG9258		47.93	0.78	17.70	9.76	9.13	12.11	2.40	0.01	1494
VG9259		47.95	0.78	17.72	9.75	9.12	12.12	2.37	0.02	1493
VG9938	Tjörnes Fracture Zone	48.33	1.19	16.20	10.29	9.03	12.86	2.06	0.03	1525
TR-139-1D-1		48.41	1.14	16.03	10.20	9.10	12.86	2.04	0.03	1522
VG9967		48.14	1.19	16.32	10.13	9.13	12.96	2.11	0.03	1513
VG9968		48.51	1.18	16.17	10.03	9.10	12.84	2.15	0.03	1512
VG9969		48.43	1.18	16.23	10.07	9.06	12.93	2.08	0.03	1514
VG1959	Juan de Fuca ridge	47.63	0.83	18.01	10.22	9.11	11.96	2.18	0.05	1517
VG1960		47.03	0.82	17.82	10.21	9.66	12.27	2.17	0.03	1510

Compositions are normalized to 100 wt%.

[a] T_P are calculated with PRIMELT2 software (Herzberg and Asimow, 2008) assuming a mantle source equal to peridotite DMM1 (Wasylenki et al., 2003; Mg# = 89.9) and an accumulated fractional melting process (see Appendix 2).

Table S4. Major-element compositions of MORB AII107-7 20-3 and of the PRIMELT2[a] Model Primary Magma (MPM) (wt%).

	AII107-7 20-3	MPM
SiO_2	49.89	49.51
TiO_2	0.62	0.60
Al_2O_3	17.27	16.64
FeO^T	7.47	7.58
MgO	10.05	11.43
CaO	13.05	12.58
Na_2O	1.64	1.58
K_2O	0.05	0.04
T_P[b]		1353
Melt fraction[c]		0.143
Ol-Mg#[d]		0.907

[a] Herzberg and Asimow (2008)

[b] Mantle potential temperature (^oC)

[c] Melt fraction of peridotite DMM1 for the case of accumulated fractional melting.

[d] Mg-number of olivine to crystallize from the primary magma at 1 atm.